A Cost-Effective Wideband Switched Beam Antenna System for a Small Cell Base Station

Petros Bantavis, Christos I Kolitsidas, Tzihat Empliouk, Marc Le Roy, B. Lars G. Jonsson, George. A Kyriacou

A Cost-effective Wideband Switched Beam Antenna System for a Small Cell Base Station

Petros I. Bantavis, Christos I. Kolitsidas, *Member, IEEE,* Tzihat Empliouk, Marc Le Roy, *Member, IEEE,* B. L. G. Jonsson and George A. Kyriacou *Senior Member, IEEE*

***Abstract*—A wideband switched beam antenna array system operating from 2 to 5 GHz is presented. It is comprised of a 4×1 Vivaldi antenna elements and a 4×4 Butler matrix beamformer driven by a digitally controlled DP4T RF switch. The Butler matrix is implemented on a multilayer structure, using 90° hybrid couplers and 45° phase shifters. For the design of the coupler and phase shifter we propose a unified methodology applied, but not limited, to elliptically shaped geometries. The multilayer realization enables us to avoid microstrip crossing and supports wideband operation of the beamforming network. To realize the Butler matrix we introduce a step by step and stage by stage design methodology that enables accurate balance of the output weights at the antenna ports to achieve stable beamforming performance. In this work we use a Vivaldi antenna element in a linear four element array, since such element supports wideband and wide-scan angle operation. A soft condition in the form of corrugations is implemented around the periphery of the array, in order to reduce the edge effects. This technique improved the gain, the side lobes and helped to obtain back radiation suppression. Finally, impedance loading was also utilized in the two edge elements of the array to improve the active impedance. The proposed system of the Butler matrix in conjunction with the constructed array can be utilized as a common RF front end in a wideband air interface for a small cell 5G application and beyond as it is capable to simultaneously cover all the commercial bands from 2 to 5 GHz.**

***Index Terms*—Wideband, Butler matrix, RF front end, 5G, Vivaldi array, soft surface, edge impedance loading, small cell.**

I. Introduction

MODERN wireless communications are driven by high quality end user experience providing high data rates, low latency and extended coverage. It is predicted that with the massive deployment of the Internet of things (IoT), the number of connected devices will increase exponentially. Network densification, [1], conjointly with heterogeneous networks (HetNets) will be in the heart of future wireless networks offering increased network capacity and spectral aggregation, [2]. Additionally, exploiting spatial multiplexing we can further increase the network capacity and offer higher signal-to-noise ratio (SNR) by focusing the RF power to the desired direction. Small base stations, [3], are in the center of the emerging next generation wireless networks playing an instrumental role to the aforementioned demands. Small cell base stations due to their foreseen massive deployment should also be very cost effective and budget friendly devices.

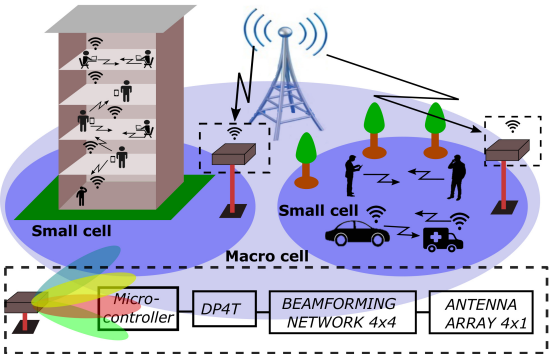

Fig. 1: Illustration of dividing data traffic into macro and small cells and the block diagram of the proposed system.

Recent works, [4], [5], have shown the potential of switched beam systems based on a Butler matrix, [6]. These works have been developed for the 60 GHz ISM band that can accommodate high data rates but with increased path loss. The resulted beamforming in the 60 GHz band will be utilized to electrically optimize the line of sight link. In [7], a 2×2 circularly polarized array with a Butler matrix capable to operate in about 48% bandwidth was presented. Slomian *et.al.* in [8] provided an array configuration with a Butler matrix capable for dual linear and dual circular polarization operating in 5.2 - 5.4 GHz. In both approaches the bandwidth was limited in less than 50% with severe impact on the second approach. A narrow band Butler matrix integrated with a patch antenna array is presented in [9]. In [10], wider bandwidth was achieved, however only simulated results are presented.

A wideband switched beam antenna system that will act as an RF air interface and will be software defined is proposed. Either a universal software radio peripheral (USRP) or a micro-controller (μC) can be used to control electronically the beamforming network. The USRP is proposed to evaluate the whole system through lab experiments, however a micro-controller is the best candidate for a massive implementation. Integrating an analogue RF switched beam system with a micro-controller offers the advantage of low cost and complexity with spatial multiplexing capabilities. The proposed

Petros. I. Bantavis was with the Lab-STICC at the university ENSTA-Bretagne in Brest, France. Now he is with institut d' electronique et de Telecommunications de Rennes, Universite de Rennes 1, e-mail (petros.bantavis@univ-rennes1.fr).

Christos I. Kolitsidas and B. L. G. Jonsson are with with the Department of Electromagnetic Engineering, School of Electrical Engineering, KTH Royal Institute of Technology, SE-100 44, Sweden. e-mail: (chko@kth.se).

Tzihat Empliouk and Georgios. A. Kyriacou are with the Microwave Laboratory, School of Electrical Engineering, Democritus University of Thrace, Xanthi, Greece. e-mail: (gkyriac@ee.duth.gr).

Marc Le Roy is with Lab-STICC at Université de Bretagne Occidentale (UBO) in Brest, France. e-mail: (marc.leroy@univ-brest.fr)

This article has been accepted for publication in a future issue of this journal, but has not been fully edited. Content may change prior to final publication. Citation information: DOI 10.1109/TAP.2018.2874494, IEEE Transactions on Antennas and Propagation

system presented in Fig. 2 is comprised of a 4×1 Vivaldi linear array fed by 4×4 Butler matrix connected to Double Pole Four Throw (DP4T) switch. The system will be controlled by a μC and have a single transmit/receive chain. This set up can offer full duplex capabilities. In this way the analogue beamforming of the Butler matrix and the digital capabilities of the μC are exploited resulting in a hybrid system. Since only one μC is required for the proposed system with only one full duplex channel, the cost is significantly reduced. The system is operating from 2 to 5 GHz providing more than one octave of usable bandwidth.

Wideband beam forming networks have already been proposed in literature as a base of switched beam systems and they have been implemented as single layer or multilayer structures. Single layer wideband Butler matrix structures have been introduced in [11], [12] where tapered line directional couplers and Schiffman phase shifters were used to implement the Butler matrix. Wide bandwidth was achieved but with the penalty of larger physical size. Several implementations of Butler matrices have adopted the multilayer slot coupled technology which was originally proposed in [13], [14] for the implementation of the required 90° hybrids and phase shifters. In [15], [16] this concept was extended into elliptically shaped geometrical structure, whereas in [17] a variation of the rectangular aperture slot coupler was presented that eliminated the magnitude rippling on the transmission coefficient. A hexagonal shaped approach was adopted in [18] and a wideband Butler matrix was designed, implemented and measured. In [19], a trapezoidal shaped geometry was introduced for the implementation of a wideband Butler matrix and only simulated results were presented for the corresponding beam performance. The last two approaches used more a brute force technique to select the corresponding geometries and no theoretical motivation or explanation was adequately provided for the design procedure of the different geometrical shapes.

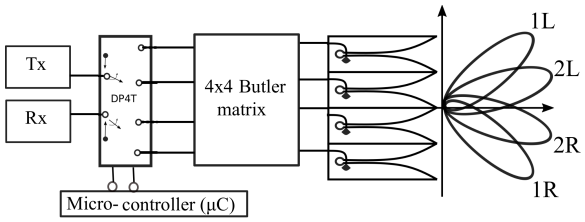

Fig. 2: The hybrid switched beam system block diagram.

In our previous works, [20], [21], we have focused on developing switched beam system for Ultra Wide Band (UWB) applications. In [22] we have presented an early version of the proposed system. Lower frequency bands and especially the sub 6 GHz communication bands have received little to no attention for small base stations as this requires challenging wideband or multiband RF circuitry development and large dimensions due to the corresponding wavelength. Due to the required backwards compatibility with the current wireless communication systems increased attention is expected to the sub 6 GHz frequencies for small cell base stations. Next generation wireless communication systems are expected to extend the capabilities but continue the support of the current systems. An illustration of the application of small cell base stations can be depicted as in Fig. 1, where small cells can be deployed on buildings or high traffic areas.

TABLE I: Ideal complex excitation currents at the antenna array elements.

BEAMS	ANT1	ANT2	ANT3	ANT4
1L	$1\angle 0^\circ$	$1\angle 135^\circ$	$1\angle -90^\circ$	$1\angle 45^\circ$
2L	$1\angle 0^\circ$	$1\angle 45^\circ$	$1\angle 90^\circ$	$1\angle 135^\circ$
2R	$1\angle 0^\circ$	$1\angle -45^\circ$	$1\angle -90^\circ$	$1\angle -135^\circ$
1R	$1\angle 0^\circ$	$1\angle -135^\circ$	$1\angle 90^\circ$	$1\angle -45^\circ$

The originality of this work refers to the design, fabrication and testing of an integrated wideband switched beam phased array system. We present a system in the sub 6 GHz band with a 4×4 Butler matrix and a 4×1 electrically connected Vivaldi array. In section II, we introduce the design methodology and we propose the unified theoretical approach on the design of multilayer 90° wideband hybrids and phase shifters. This approach was applied in the elliptically shaped geometry but it can easily be extended in any other geometrical shape. The overall Butler matrix design is also presented in this section. The proposed Butler matrix is connected with a linear 4×1 linear Vivaldi array that is introduced in section III. The combination of edge impedance loading and a soft condition at the array's periphery are utilized to achieve the wideband characteristics of such a small array. The overall system performance is presented in section IV. Finally, the conclusions of this work are summarized in section V.

II. Design methodology

A. 4×4 *Butler matrix design*

Butler matrix is one of the most widespread analogue beamforming networks. It is composed of N inputs (excitation ports) and N outputs (antennas ports) where $N = 4$. The number of couplers is equal to $(N/2)\log_2(N)$ and the number of phase shifters to $(N/2)[\log_2(N) - 1]$, [6]. Exciting one of its N inputs produces uniform amplitudes at the output ports with a phase difference $\Delta\phi$. This phase difference between the output ports is different for every input port excitation and at the same time it is the factor that steers the beam in the desired direction in space. As a result of the uniform excitation currents the radiation field is of the form $\sin x/x$. Exciting the input ports of a $N = 4$ matrix separately, four orthogonal beams are produced, so there is no significant interference between the consecutive beams. The operation of the Butler matrix and the resulting ideal excitation power vectors can be summarized in TABLE I.

In order to induce wideband characteristics the present Butler matrix consists of multilayer couplers and phase shifters. Another advantage of the multilayer technology is that it avoids undesired line crossings. Thus, a compact and wideband beamforming network in the sub 6 GHz communication band from 2 to 5 GHz as depicted in Fig. 2 is designed, fabricated and tested. In Fig. 3(a) the schematic of a 4×4 Butler matrix is depicted and it consists of four 90° hybrid couplers and two 45° phase shifters. This approach is extended for both the hybrid couplers and phase shifters, especially when

implemented with elliptical patches and slots. This multilayer technology besides the wideband operation overcomes the usual problem of interconnecting line crossings encountered in printed microstrip Butler matrices. An indicative layout geometry of the technology is illustrated in Fig. 3(b) where the continuous and dashed lines represent different layers. It is clear that no line crossing occurs in the same layer. In Fig. 3(b) it is shown the corresponding physical implementation. In Fig. 3(c) the multilayer configuration of the coupler is depicted, where two elliptical patches are printed on the top and bottom surfaces of two grounded substrates pressed back-to-back at their common ground plane. An elliptical slot is etched on their common ground plane which is oriented orthogonally to the elliptical patches. To build the respective prototype the top and bottom substrates are fabricated separately and then pressed and glued together.

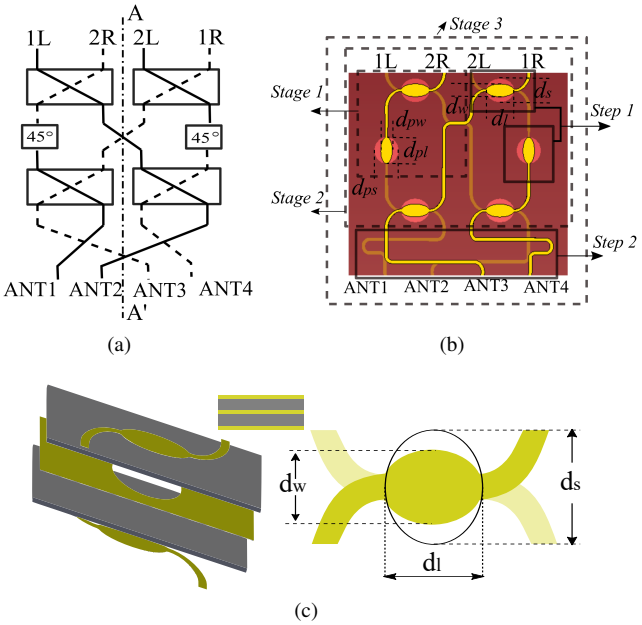

Fig. 3: (a) Butler matrix block diagram with the continuous and dashed lines defining different layers (b) Top layered view of the developed Butler matrix where the middle copper layer is with brown color and the top bottom copper layers with light dark and light yellow shades. The denoted dimensions in mm: $d_s = 13.7$, $d_l = 14.9$, $d_w = 6.1$, $d_{ps} = 13$, $d_{pl} = 13.8$, $d_{pw} = 5.9$. (c) 3D layered illustration of the hybrid coupler and top perspective same as (b).

The final layout implementation is shown in Fig. 3(b) where the three distinctive layers are visible. The dimensions of the coupler and phase shifter that are integrated in the Butler matrix are shown in Fig. 3(b). A step by step and a stage by stage design procedure is proposed for the Butler matrix design. The design is divided in two steps and three stages as indicated in Fig. 3(b). The first step is to design the individual subnetworks, which are the hybrid coupler and the phase shifter of the Butler matrix. After the successful design of the two individual components the coupler is connected with the phase shifter resulting in a two port network. At this stage the components are numerically optimized again to achieve optimal cooperative performance. Next, at stage 2 the Butler matrix is designed. The magnitude and phase behavior of this network are evaluated and numerically optimized. The design procedure continues with the second step, (see Fig. 3(b)), where the equiphased transmission line network is designed separately. This line network will align and order in sequence the Butler matrix output ports to correspond to the linear antenna array ports enabling their integration. Finally, in the third stage the circuitry from the two previous stages is integrated and the overall performance of the final Butler matrix is evaluated.

B. Subnetworks

The adopted technology for the hybrid couplers and phase shifters consists of three conductive layers interleaved with two dielectric layers as shown in Fig. 3(b). The top and bottom layers are coupled through an aperture slot that is located in the middle layer. The coupling phase and bandwidth are controlled by the shape of the two conductive patches and the slot. Rogers 4003C with thickness h=0.813 mm is used for a substrate as a design material that provides a good compromise between losses and cost for RF circuit. The phase shifters adopted in this work are based on the same principle as the hybrid couplers. However, they provide a constant phase-shift versus frequency with respect to a corresponding uniform transmission line.

In this work we propose a unified design methodology for the 90° hybrid coupler and phase shifter based on [15], [16] which in turn are based on the original work from [13] since the designs share a similar geometrical cross section. The coupling coefficient can be calculated as:

$$C = \frac{Z_e - Z_o}{Z_e + Z_o} \tag{1}$$

where Z_e and Z_o denote the even and odd mode characteristic impedances. The feeding microstrip line characteristic impedance is calculated using the geometrical mean $Z_0 = \sqrt{Z_e Z_o}$. The impedances Z_e, Z_o are derived from [13] using the image theory as:

$$Z_e = \frac{60\pi}{\sqrt{\epsilon_r}} \frac{K(k_1)}{K'(k_1)} \tag{2}$$

$$Z_o = \frac{60\pi}{\sqrt{\epsilon_r}} \frac{K'(k_2)}{K(k_2)} \tag{3}$$

where $K(k)$ is the elliptical integral of first kind and $K'(k)$ its complementary given by $K'(k) = K(\sqrt{1-k^2})$. This ratio of elliptic integrals can be approximated either numerically or using the formulas given in [13]. The elliptic modulus k_1, k_2 are given based on the geometrical characteristics as follows:

$$k_1 = \sqrt{\frac{\sinh^2(\pi^2 E_s/(16h))}{\sinh^2(\pi^2 E_s/(16h)) + \cosh^2(\pi^2 E_w/(16h))}} \tag{4}$$

$$k_2 = \tanh(\pi^2 E_w/(16h)) \tag{5}$$

where $E_s \in \{d_s, d_{ps}\}$ and $E_w \in \{d_w, d_{pw}\}$ with respect to the notation of Fig. 3(b) and Fig. 3(c). A $\pi/4$ multiplier has

been added when compared to the original formulas from [23]. This multiplier indicates the area ratio between a rectangle, A_{rect}, with sides (a, b) and the corresponding inscribed ellipse with area A_{ell}, as $A_{ell/A_{rect}} = (\pi ab/4)/(ab) = \pi/4$. This $\pi/4$ multiplier accounts for the ellipticity of the adopted geometry. An additional step is required for the phase shifter. Its corresponding phase shift when referenced to a microstrip line is given in [16]:

$$\Delta\phi = \pi/2 - \arctan\left[\frac{\sin(\beta_{eff}d_{pl})}{\sqrt{1-C^2}\cos(\beta_{eff}d_{pl})}\right] + \beta_{ms}l_{ms} \quad (6)$$

where $\beta_{eff} = \beta_0\sqrt{\epsilon_r}$, β_{ms} is the corresponding microstrip propagation constant, $d_{pl} = \lambda_{ms}/4 = d_l$ with λ_{ms} the effective microstrip wavelength and l_{ms} the microsrip line reference length. Equation (6) reveals that there are two degrees of freedom to achieve the desired phase shift, the coupling coefficient and the l_{ms}. Hence in this particular case the coupling coefficient C of the phase shifter is chosen based on the corresponding length required from the layout. This concludes the proposed unified approach for the design of the elliptically shaped aperture coupled phased shifter and hybrid coupler. Our proposed unified design methodology is not limited to elliptically shaped coupling geometries and can easily be extended to other coupling geometries simply by modifying accordingly the area ratio. Calculating such multiplier for any other geometry such as diamond shaped or hexagonal can provide a priori analytical estimates for the corresponding physical dimensions. The wideband characteristics and the small physical footprint of the coupler and the phase shifter are attributed to the folded aperture coupling occurring in different layers.

1) Prototypes Construction: For the construction process silver epoxy was used in order to connect the two printed circuit boards (PCB) layers. The ground metalization is retained in both PCB layers to avoid via padding for the coaxial connector and manufacturing ease. Only board routing is required with this methodology. The first step was to spread this epoxy over the whole surface of one layer and then press together the metalized layers (ground planes) mechanically. During the pressing, the PCB is heated for 10 minutes at 100° C. This heating helps the epoxy to get similar conductivity as the copper and the layers adhere effectively without air-bubbles trapped in between.

2) Hybrid Coupler: The first constructed subnetwork is the 90° hybrid coupler obtained from the overall design process described above. Since the integrated design is evaluated the deviation from the ideal results will indicate the difference resulted from the interconnection of individually designed components. Starting the equations (1)-(5) the initial ellipses dimensions denoted in Fig. 3(b) (values in mm) $d_s = 8.1$, $d_l = 12.99$ and $d_w = 6.1$ are obtained. Ideally, exciting port 1, as designated in the inset of Fig. 4 the coupler equally divides the power into ports 2 and 3 with a 90° phase difference, while port 4 remains isolated. The simulation and measurement results for the magnitude of the constructed coupler are depicted in Fig. 4. An acceptable variation of ± 0.75 dB from the ideal value of -3 dB is observed in the 2-5 GHz band of interest, whereas the reflection coefficient and the isolation are kept below -18 dB.

3) Phase Shifter: The other internal component of the Butler matrix is the phase shifter. A 4×4 Butler requires two phase shifters with $\Delta\phi = 45^\circ$ as illustrated in Fig. 3(a). A differential phase shifter is utilized which is based on the same multilayer technology by open ending and removing the transmission lines from ports 3 and 4 of the hybrid coupler. Using equations (1) - (6) we obtain the initial values in mm $d_{ps} = 8.92$, $d_{pl} = 12.99$ and $d_{pw} = 6.22$. This phase shifter is able to provide constant phase shift when referenced to a corresponding transmission line. The topology of the Butler matrix has this property inherently since a transmission line is required to connect the two remaining ports (see Fig. 3(a)) of the first stage of hybrid couplers. These initial dimensions are optimized to achieve the required constant phase shift throughout the bandwidth of the operation. The constructed phase shifter and the referenced line are depicted in the inset of of Fig. 5. Excellent agreement between simulation and measurements of the designed subnetwork is illustrated in Fig. 5. Very low losses (< 1 dB) are also observed in the band of interest.

In Fig. 6 the phase responses for both the coupler and the phase shifter are illustrated. For the coupler the phase difference between the output ports 2, 3 when port 1 is excited is illustrated (inset of Fig. 4), whereas for the phase shifter the achieved phase difference with respect of the reference transmission line $\Delta\phi = \angle S_{21} - \angle S_{34}$ is depicted in Fig. 5. Very good agreement between the simulation and the measurements and the ideal value is observed for the sub-band 2.5-4 GHz. For the low and the high end of the band, higher but acceptable deviations up to 5° are observed. The deviations can also be traced in the manufacturing process of the subnetworks where we utilized a milling process for this implementation. The milling process will not protect the copper of the PCB of being contaminated with particles that could potentially result in higher resistivity of the ground connection. The milling process can also affect the thickness of the substrate which can impact the phase. The final Butler matrix is constructed using etching process and a semi-clean room environment to avoid the aforementioned issues.

C. Butler Matrix Network Implementation and Measurements

After the implementation and verification of the two key components of the Butler matrix, the procedure continues with the implemented network verification. An ideal Butler matrix will equally divide the power from an input port and depending on the activated port, four different sets of phase sequences with $\Delta\phi = \pm 135^\circ$ and $\pm 45^\circ$ are obtained corresponding to four respective beams.

The final constructed Butler matrix is depicted in Fig. 7 and has overall dimensions 150 mm$\times$ 110 mm. Emphasis has been given to the outputs of the Butler matrix to be placed in sequential order and thus be ready to connect with the antenna array. Furthermore, the distance between the output ports is set to be same as for the designed linear Vivaldi array that will be described in section III. The latter step has been taken so that

This article has been accepted for publication in a future issue of this journal, but has not been fully edited. Content may change prior to final publication. Citation information: DOI 10.1109/TAP.2018.2874494, IEEE Transactions on Antennas and Propagation

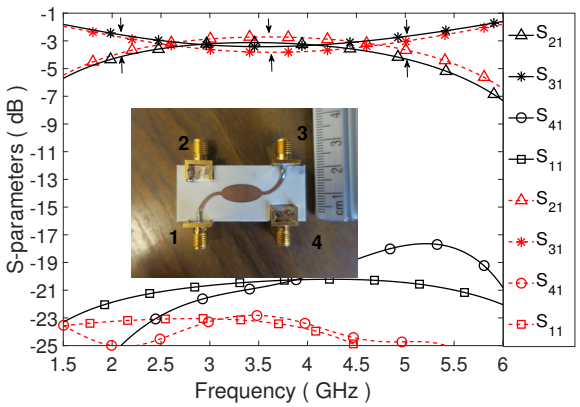

Fig. 4: Constructed 90° hybrid coupler with the corresponding magnitude measurements. The continuous (–) line denotes the simulated and the dotted (- -) the measured results.

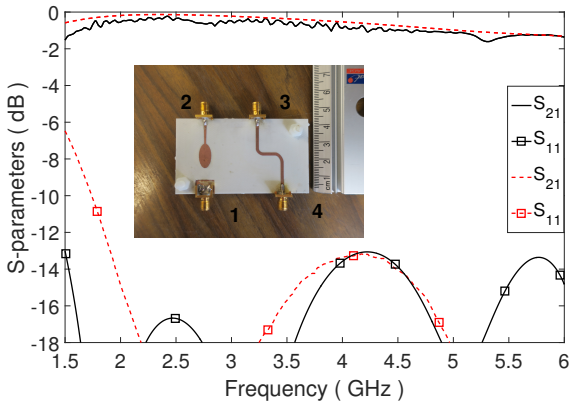

Fig. 5: Constructed 2×2 sub-network of Butler matrix - Phase shifter $45°$ and the reference line where the continuous (–) line denotes the simulated and the dotted (- -) the measured results.

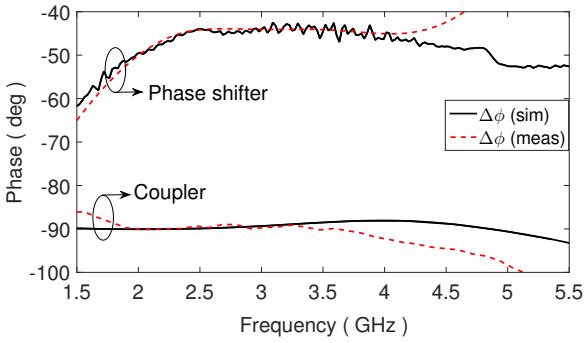

Fig. 6: Phase difference between the output ports of the coupler of Fig. 4 and the phase shifter of Fig. 5.

the Butler matrix and the antenna array can be integrated in a single PCB board if so required. In this work they have been separately constructed for ease of measurements and result clarity.

Butler matrix has a plane of reflection symmetry, as shown

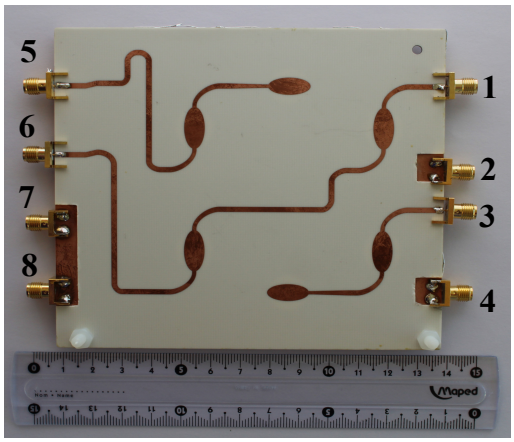

Fig. 7: Constructed prototype of 4×4 Butler matrix.

in Fig. 3(a), thus simulated and measured results are presented for the magnitude only when port 1 is excited and phase shifts exciting ports 1 and 2. In Fig. 8, the insertion loss S_{51}, S_{61}, S_{71} and S_{81} are shown. The measured results appear to be more lossy than the simulated ones by approximately 0.75 dB. However, apart from the losses the magnitude values appear grouped for each frequency point. This implies that a response close to the theoretical uniform aperture illuminated beam should be obtained. Namely, all path losses are increased by 0.75 dB, thus yielding again the same signal amplitudes at the outputs, almost uniformly degraded by 0.75 dB. The other important characteristics are the reflection coefficient at port 1 and the isolation coefficient between the remaining input ports 2, 3 and 4. These results are depicted in Fig. 9 which verifies that all the coefficients are below -12 dB, thus good matching and isolation has been achieved.

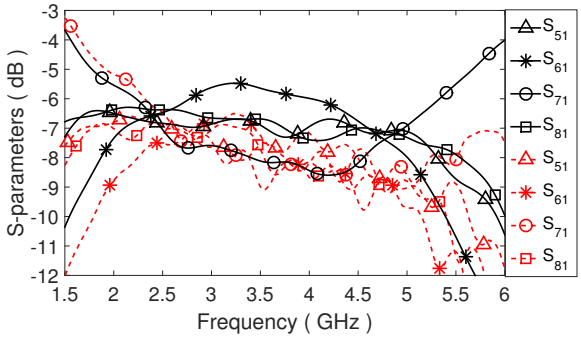

Fig. 8: Insertion losses of Butler matrix exciting port 1. The continuous (–) line denotes the simulated and the dotted (- -) the measured results.

To fully characterize the performance of the Butler matrix the phase difference between the output ports needs to be verified. Since the network is fully symmetric, results for only ports 1 and 2 are illustrated. When port 1 is excited, $\Delta\phi = -135°$ is expected between the output ports. Indeed as it is depicted in Fig. 10 the corresponding results from both simulation and measurements verify that the mean value of the phase difference is around $-135°$ for the frequency

This article has been accepted for publication in a future issue of this journal, but has not been fully edited. Content may change prior to final publication. Citation information: DOI 10.1109/TAP.2018.2874494, IEEE Transactions on Antennas and Propagation

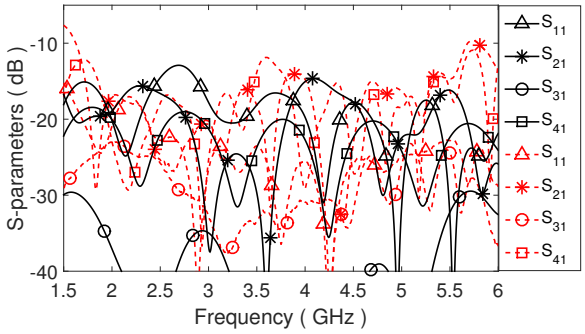

Fig. 9: Reflection and isolation coefficients of Butler matrix exciting port 1. The continuous (–) line denotes the simulated and the dotted (- -) the measured results.

band 2-5 GHz with a mean deviation of $\pm 4^\circ$. Similarly, a phase difference of $\Delta\phi = -45^\circ$ is expected when port 2 is excited. The respective performance for port 2 is depicted in Fig. 11. A maximum $\pm 4^\circ$ fluctuation from the ideal values is achieved for either excitation. This variation is small enough to avoid beam stitching so that the expected beam performance will be obtained. Similar results for the magnitude and phase are verified for the remaining ports. It is noticeable that the measured results are not well aligned with the simulated in Fig. 8 - Fig. 11. This misalignment comes from our in-house manufacturing process. When the layers were stacked with the conductive epoxy the higher tolerances affected the coupling slot.

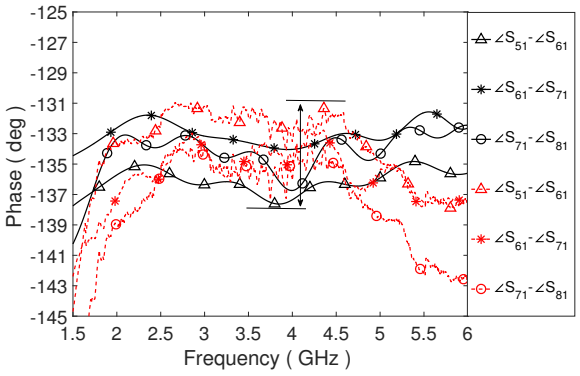

Fig. 10: Phase difference of the consecutive output ports of Butler matrix exciting port 1. The continuous (–) line denotes the simulated and the dotted (- -) the measured results.

III. Linear Vivaldi Array Design

The Butler matrix is integrated with a 4×1 linear array. As an array element, an exponential tapered slot antenna (TSA) or Vivaldi [24] has been selected for its wideband and wide-scan performance. The Vivaldi antenna element performs exceptionally in terms of cross polarization in the two principal E- and H-planes whereas its performance deteriorates significantly in the inter-cardinal (D-) plane. However, in this application only E-plane scan is utilized hence the motivation of the Vivaldi as a radiating element in this work.

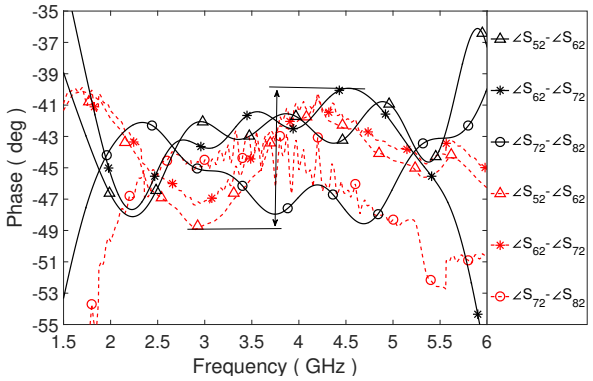

Fig. 11: Phase difference of the consecutive output ports of Butler matrix exciting port 2. The continuous (–) line denotes the simulated and the dotted (- -) the measured results.

For the array design we consider as maximum frequency of operation $f_{max} = 6$ GHz. This implies interelement distance d=24.8 mm that corresponds to approximately $\lambda_0/2$ at middle frequency. For the element design a single element is placed as a unit cell. We assume periodicity on the E-plane of the element and free space conditions on the remaining boundaries. This will provide an initial approximation on the design as the Vivaldi elements are electrically connected, hence tightly coupled. However, the goal is to design a 4×1 linear array and this will provide only a starting point.

The design of the Vivaldi array is depicted in Fig. 12. Two methodologies are invoked during the design process to further improve the performance of the array in terms of radiation characteristics and impedance matching. For the radiation characteristics we employ a soft condition in the surrounding area of the array [25]. The soft condition is implemented in the classic form of corrugations as illustrated in Fig. 12(a). The geometrical ridge resulting from the corrugations will zero the transverse electric field $E_t = 0$. The corrugations will act as STOP condition for the fields to radiate from the array edges. The soft surface inserts a high impedance path for the current following the edges of the array. The impact of the soft condition in the radiating pattern in terms of co and cross (x) polarization (pol) is depicted in Fig. 13. It is observed that the co-pol gain is increased by 1 dB and the x-pol is decreased in the main lobe half-space along with the average back radiation. In addition, since this is a small linear array, to improve the impedance behavior of the small array impedance loading has been utilized to the two edge elements compared to the inner-ones as indicated with the different dimensions in Fig. 12(b) and Fig. 12(c). This compensates the fluctuation on the impedance caused by the remaining edge scattering and the electromagnetic environmental difference in terms of mutual coupling. This methodology can be considered as a hardware implementation of mutual coupling compensation, [26], where the difference in mutual coupling on the edge elements is compensated by impedance loading. To calculate this loading, the slot impedance of the Vivaldi in the presence of mutual coupling was evaluated. This numerical evaluation resulted in 7 Ohm higher impedance for the edge-outer elements. Its

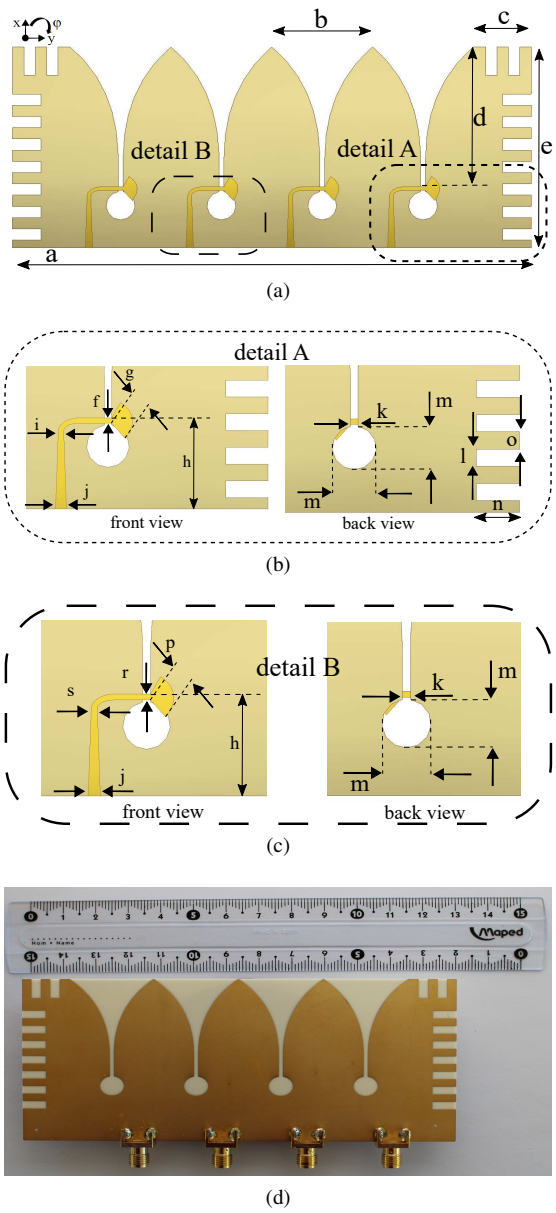

Fig. 12: Vivaldi array (a) middle and (b) edge stub (c) prototype. Dimensions in mm: a=127.6, b = 24.8, c=14.2, d=36, e=50, f=0.9, g=3.4, h=14, i=0.9, j=1.8, k=1.2, l=2.8, m=7, n=7, o=2.8, r=1.1, s=1.3, p=3.7

specific value was estimated through a de-embedding process in the finite array structure that evaluated the impedance at the middle of the slot. The edge elements were in turn matched to the new acquired impedance and tested to the Butler matrix output vectors. All elements have been matched to an input impedance of 50 Ohm for a standard coaxial connector to be used during the measurement process.

The final constructed array is illustrated in Fig. 12(d) with overall dimensions 133 mm×80 mm and its corresponding detailed dimensioning is shown in Fig. 12(a) and Fig. 12(b). The simulated and measured active reflection coefficient of the array is depicted in Fig. 15. The measured active reflection coefficient is evaluated by obtaining the full scattering matrix of

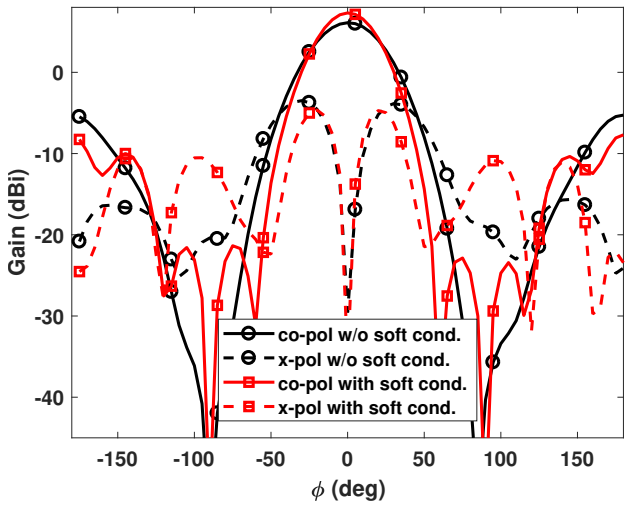

Fig. 13: Co-polarization and cross-polarization comparison of the Vivaldi array with and without the soft surface for the broadside beam ($\phi = 90°$) at 3 GHz.

the array and post-processing utilizing the following equation (7).

$$\Gamma_m(\theta_0) = \sum_{n=1}^{N} S_{mn} e^{jka\sin(\theta_0)(m-n)} \tag{7}$$

The simulated and measured S-parameters for port 1 and port 2 of the array are illustrated in Fig. 14(a) and Fig. 14(b) respectively. Very good agreement between simulated and measured results is observed. The embedded S-parameters are in turn post-processed using equation (7) and the active reflection coefficients for the beam 1R are depicted in Fig. 15. The measured and simulated results are in good agreement and the level of the active reflection coefficient is below -10 dB for the whole band of operation. The active impedance matching results further motivates our approach for impedance loading as all ports achieve the same bandwidth performance. A similar post processing procedure is followed when the other input ports 2, 3, 4 are activated. In all cases the active input reflection coefficients are retained below -10 dB in the 2-5 GHz band for both simulated and measured results.

The combination of edge impedance loading at the outermost element of the array and the well-established soft condition on the array's periphery constitute part of the introduced design methodology of this switched beam antenna system.

IV. System Assembly and Performance

At this point the two components have been successfully designed. However, it is important to evaluate the overall performance of the system fully assembled. Since the ports of the Butler matrix and the ports of the Vivaldi array have already been designed to be collocated, the two networks can easily be cascaded. The S-parameters for the two cascaded networks are illustrated in Fig. 16. In effect these cascaded S-parameters contain the active array impedance and the performance of the Butler matrix. Very good agreement between the simulated and the measured results is shown as well as symmetry is observed for the cascaded network S-parameters between S_{11}, S_{44} and

This article has been accepted for publication in a future issue of this journal, but has not been fully edited. Content may change prior to final publication. Citation information: DOI 10.1109/TAP.2018.2874494, IEEE Transactions on Antennas and Propagation

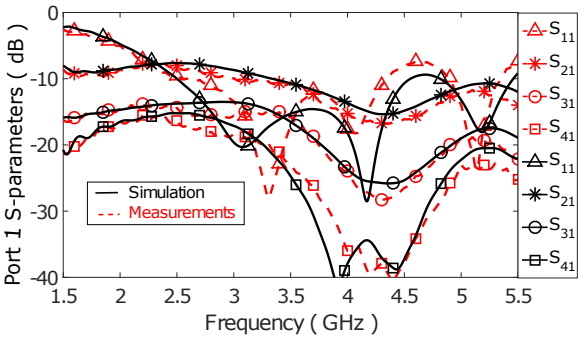

(a)

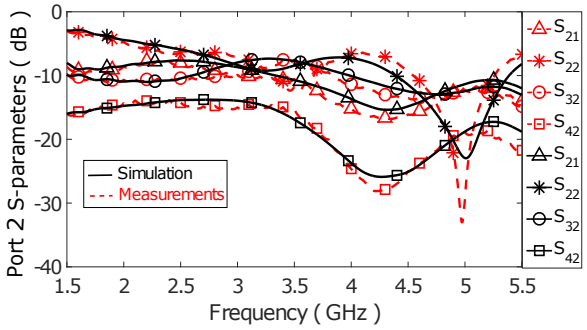

(b)

Fig. 14: S-parameters exciting the ports (a) 1 and (b) 2 of the Vivaldi array.

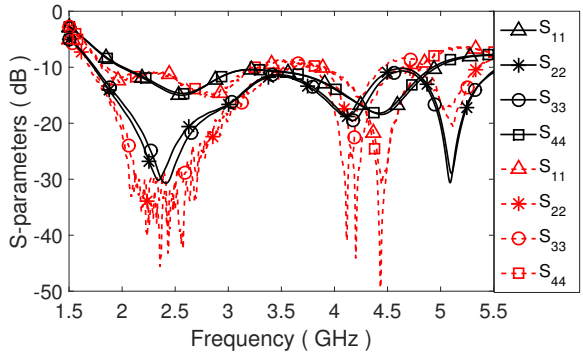

Fig. 15: Active S- parameters of Vivaldi antenna array for the beam 1R. The continuous (–) line denotes the simulated and the dotted (- -) the measured results.

S_{22}, S_{33} since they are almost identical. This symmetry of the S-parameters implies good overall construction.

By exciting the input ports of Butler matrix separately four orthogonal beams are produced. In the developed wideband Butler matrix we achieve constant phase difference at its outputs across the frequency. This will impact the beam behavior as the maximum of each beam ϕ_{max} will have a dispersive behavior according to $\phi_{max} = \arcsin(\Delta\phi\ \lambda/2\pi d)$ where $\Delta\phi$ is the Butler matrix phase difference for each excitation vector.

The simulated and measured radiation patterns of the system at 2, 3, 4 and 5 GHz are presented in Fig. 17. The presence of

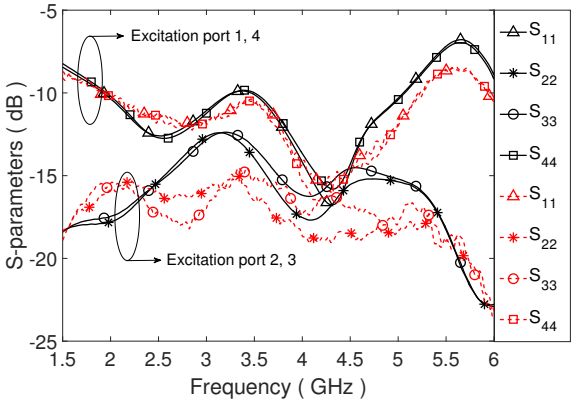

Fig. 16: Cascaded S-parameters of Vivaldi antenna array exciting separately the input ports of Butler matrix. The continuous (–) line denotes the simulated and the dotted (- -) the measured results.

the Butler matrix and the cables resulted in spurious radiation to be emitted. This was observed during the far field system measurements. It was observed that in all cases the outermost beams deviate significantly from the simulations. This was attributed to our measurement set up that required equal length and phase stable cables to connect the Butler matrix and the Vivaldi array (see Fig. 18(c)). To illustrate this, the embedded patterns of the array were also separately measured. These embedded patterns were post-processed according to equation (8) to obtain the array's far field pattern. In equation (8) we denote as $AP(\theta, \phi)$ the resulted array pattern, with w_n the weight given to each element and with E_n the corresponding embedded element pattern.

$$AP(\theta, \phi) = \sum_{n=1}^{N} w_n E_n(\theta, \phi). \tag{8}$$

In equation ((8)) we applied the measured Butler matrix weights w_n and the embedded element patterns $E_n(\theta, \phi)$ of each element and we calculate the radiation pattern of the array for the frequencies 2, 3, 4 and 5 GHz. The simulated and post processed measured results are in very good agreement. In the presented system level measurements, the cables and the Butler matrix were covered with absorbers resulting in poor back lobe accuracy. This is visible in all system measured radiation patterns. Exciting the Butler matrix ports corresponding to the beams 2L and 2R, side lobe level (SLL) of -12.9 dB and -13.1 dB are achieved respectively. Exciting the corresponding ports 1L and 1R we have measured SLL of approximately -12 dB whereas deviation from the simulated pattern is observed.

Fig. 18(a) and Fig. 18(b) depicts the system gain versus frequency for all the beams of Fig. 2 and there is a maximum variation of 1 dB between simulated and measured results. The system efficiency was calculated using full wave electromagnetic simulation with the Vivaldi antenna been directly connected to the outputs of the Butler matrix. The measured values of the system efficiency are extracted from the cascaded antenna array and Butler matrix network removing the impact of the connecting cables. The antenna array efficiency along

This article has been accepted for publication in a future issue of this journal, but has not been fully edited. Content may change prior to final publication. Citation information: DOI 10.1109/TAP.2018.2874494, IEEE Transactions on Antennas and Propagation

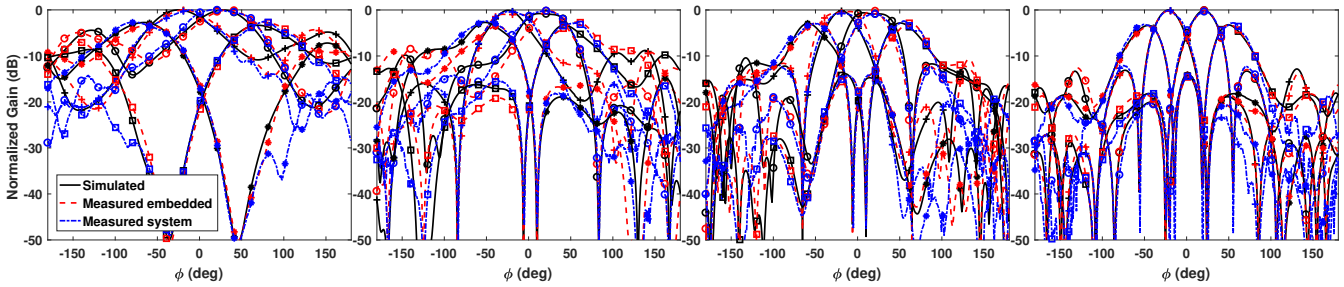

(a) f = 2 GHz (b) f = 3 GHz (c) f = 4 GHz (d) f = 5 GHz

Fig. 17: Simulated and measured radiation pattern at 2, 3, 4 and 5 GHz. The beam 1L is annotated with $*$, the 2L with $+$, the 2R with $\circ$ and the 1R with $\square$. The legend and scale on the normalized gain are the same in all graphs.

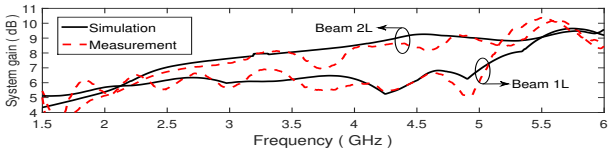

(a)

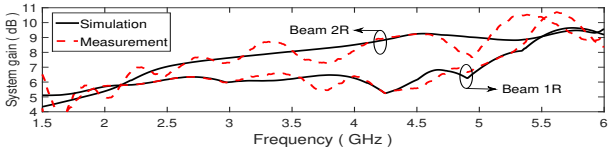

(b)

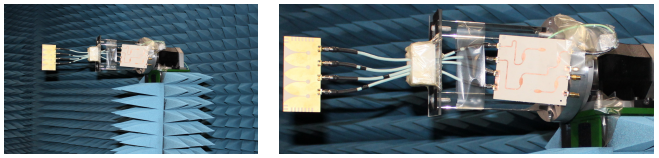

(c)

Fig. 18: (a), (b) System gain of the whole beamforming network for all the beams (2R,1R,2L,1L) of Fig. 2 (Vivaldi array and Butler matrix (c) Measurement set up in the anechoic chamber).

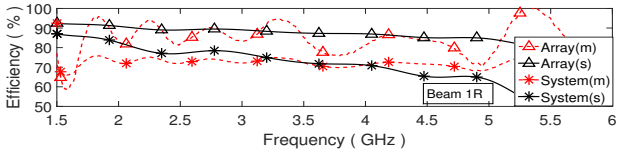

(a)

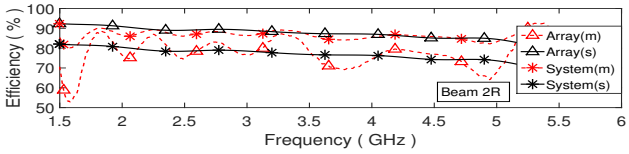

(b)

Fig. 19: Antenna array (Array) and system efficiency (System) for the beams (a) 1R and (b) 2R of Fig. 2. The notation (m) and (s) at the legends indicates the measured and simulated results respectively.

with the overall system efficiency are shown in Fig. 19(a) and Fig. 19(b) for the beams 1R and 2R from simulations and measurements. Above 80% antenna efficiency is achieved for a scanned beam and above 65% for the system efficiency. The connectors and the cables utilized in this measurement have been cascaded in the simulated data as well. It is worth to note that the system is symmetric as was indicated from the measured and simulated beam patterns, see Fig. 17, and similar behavior is shown for the beams 1L and 2L. A summary of the properties of our proposed system as well as relevant works from the literature are tabulated at the Table. II. Therein, the technology of each work is indicated in terms of single or multi-layer substrate, the overall bandwidth performance as a ratio between the high and low frequency BW $= f_h/f_l$ of operation, beam performance for a switched beam system with each design indicated, noting if simulations or measurements are present. The size of the Butler matrix is depicted in terms of the corresponding high frequency free space wavelength. It is clear that the methods adopted in this work benefit for small size and wideband system performance can be achieved.

TABLE II: Comparison of switched beam systems

	Tech.	BW	Beam perf.	Size
[10]	multilayer	3.42	yes (S)	$2.02\lambda_h \times 1.68\lambda_h$
[4]	single layer	1.12	yes (S&M)	$2.55\lambda_h \times 2.38\lambda_h$
[5]	single layer	1.12	yes (S&M)	$2.3\lambda_h \times 1.74\lambda_h$
[18]	multilayer	3.42	yes (S)	$3.03\lambda_h \times 2.36\lambda_h$
[19]	multilayer	3.42	yes (S)	$2.7\lambda_h \times 2.53\lambda_h$
This work	multilayer	2.5	yes (S&M)	$2.15\lambda_h \times 1.71\lambda_h$

V. Conclusions

A novel topology is proposed for an RF front end to be applied in small cell applications for the future generation wireless networks. A wideband 4×4 Butler matrix is implemented as a beamforming network in conjunction with a wideband 4×1 linear Vivaldi array operating from 2 to 5 GHz. The system is able to achieve four directional beams at all frequencies. The linear Vivaldi array offers improved wideband performance up to 6 GHz and can be utilized with a feed network in parallel with the proposed Butler matrix. The Butler matrix network is implemented in

multilayer technology following the stage-by-stage proposed design methodology for the critical subnetworks. This avoids any undesired microstrip cross sections and also improves the iterations of prototyping respectively. We have introduced a unified design methodology for such multilayer structures that can be expanded to any geometrical shape. Two techniques are proposed herein for the improvement of the impedance matching and the radiation pattern of the Vivaldi array. For the former an impedance loading to the outer antenna elements, while a soft condition is implemented as corrugations around the antenna periphery for the latter. Besides, the matching and the gain improvement these approaches reduced the side lobes and back radiation. Finally, the Butler matrix and the antenna array have been co-designed in the same material and the outputs or the Butler matrix have been placed in a sequential order to correspond at the antenna ports. This enabled the development of the system under the same PCB manufacturing. The multilayer design avoided all Butler matrix line crossings and minimized the overall footprint of the circuitry.

ACKNOWLEDGMENT

This work was partially financially supported by The Swedish Governmental Agency for Information Systems (VINNOVA) within the VINN Excellence center, ChaseOn through the research project Integrated Antenna Arrays. The authors thank Dr. Mathieu Cariou and Dr. Tomi Murovec in Fablab, UBO for the construction of the PCBs.

REFERENCES

[1] N. Bhushan, J. Li, D. Malladi, R. Gilmore, D. Brenner, A. Damnjanovic, R. T. Sukhavasi, C. Patel, and S. Geirhofer, "Network densification: the dominant theme for wireless evolution into 5G," *IEEE Communications Magazine*, vol. 52, no. 2, pp. 82–89, February 2014.

[2] J. G. Andrews, S. Buzzi, W. Choi, S. V. Hanly, A. Lozano, A. C. K. Soong, and J. C. Zhang, "What will 5G be," *IEEE Journal on Selected Areas in Communications*, vol. 32, no. 6, pp. 1065–1082, June 2014.

[3] D. Muirhead, M. A. Imran, and K. Arshad, "A survey of the challenges, opportunities and use of multiple antennas in current and future 5G small cell base stations," *IEEE Access*, vol. 4, pp. 2952–2964, 2016.

[4] C. E. Patterson, W. T. Khan, G. E. Ponchak, G. S. May, and J. Papapolymerou, "A 60-GHz active receiving switched-beam antenna array with integrated Butler matrix and gaas amplifiers," *IEEE Transactions on Microwave Theory and Techniques*, vol. 60, no. 11, pp. 3599–3607, Nov 2012.

[5] C. H. Tseng, C. J. Chen, and T. H. Chu, "A low-cost 60-GHz switched-beam patch antenna array with Butler matrix network," *IEEE Antennas and Wireless Propagation Letters*, vol. 7, pp. 432–435, 2008.

[6] J. Butler and R. Lowe, "Beam forming matrix simplifies design of electronically scanned antennas," *Electronic Design*, vol. 9, pp. 170–173, 1691.

[7] H. H. Tran and I. Park, "Wideband circularly polarized 2×2 antenna array with multibeam steerable capability," *IEEE Antennas and Wireless Propagation Letters*, vol. 16, pp. 345–348, 2017.

[8] I. Slomian, K. Wincza, and S. Gruszczynski, "Series-fed microstrip antenna lattice with switched polarization utilizing Butler matrix," *IEEE Transactions on Antennas and Propagation*, vol. 62, no. 1, pp. 145–152, Jan 2014.

[9] K. Wincza and S. Gruszczynski, "A broadband 4x4 Butler matrix for modern-day antennas," in *2005 European Microwave Conference*, vol. 2, Oct 2005, pp. 4 pp.–.

[10] A. Talbi, M. L. Seddiki', and F. Ghanem, "A compact 4x4 Butler matrix for UWB applications," in *2013 IEEE Antennas and Propagation Society International Symposium (APSURSI)*, July 2013, pp. 1010–1011.

[11] S. Gruszczynski, K. Wincza, and K. Sachse, "Broadband 4x4 Butler matrices utilizing tapered-coupled-line directional couplers," in *2011 MICROWAVES, RADAR AND REMOTE SENSING SYMPOSIUM*, Aug 2011, pp. 77–81.

[12] ——, "Compact broadband Butler matrix in multilayer technology for integrated multibeam antennas," *Electronics Letters*, vol. 43, no. 11, pp. 635–636, May 2007.

[13] W. Hilberg, "From approximations to exact relations for characteristic impedances," *IEEE Transactions on Microwave Theory and Techniques*, vol. 17, no. 5, pp. 259–265, May 1969.

[14] T. Tanaka, K. Tsunoda, and M. Aikawa, "Slot-coupled directional couplers between double-sided substrate microstrip lines and their applications," *IEEE Transactions on Microwave Theory and Techniques*, vol. 36, no. 12, pp. 1752–1757, Dec 1988.

[15] A. M. Abbosh and M. E. Bialkowski, "Design of compact directional couplers for UWB applications," *IEEE Transactions on Microwave Theory and Techniques*, vol. 55, no. 2, pp. 189–194, Feb 2007.

[16] A. M. Abbosh, "Ultra-wideband phase shifters," *IEEE Transactions on Microwave Theory and Techniques*, vol. 55, no. 9, pp. 1935–1941, Sept 2007.

[17] A. Moscoso-Martir, J. G. Wanguemert-Perez, I. Molina-Fernandez, and E. Marquez-Segura, "Slot-coupled multisection quadrature hybrid for UWB applications," *IEEE Microwave and Wireless Components Letters*, vol. 19, no. 3, pp. 143–145, March 2009.

[18] L. M. Abdelghani, T. A. Denidni, and M. Nedil, "Ultra-broadband 4x4 compact Butler matrix using multilayer directional couplers and phase shifters," in *2012 IEEE/MTT-S International Microwave Symposium Digest*, June 2012, pp. 1–3.

[19] O. M. Haraz, A.-R. Sebak, and S. A. Alshebeili, "Ultra-wideband 4x4 Butler matrix employing trapezoidal-shaped microstrip-slot technique," in *Wireless Personal Communications*, May 2015, pp. 709 – 721.

[20] C. I. Kolitsidas, C. S. Lavranos, and G. A. Kyriacou, "Design of a wideband RF front end based on multilayer technology," in *PIERS Proceedings, Moscow, RUSSIA*, August 19-23 2012, pp. 733 – 737.

[21] F. E. Fakoukakis, T. Empliouk, C. I. Kolitsidas, G. A. Ioannopoulos, and G. A. Kyriacou, "Ultra-wideband Butler matrix fed MIMO antennas," in *PIERS Proceedings, Prague, Czech Republic*, July 6-9 2015, pp. 2815 – 2819.

[22] P. I. Bantavis, C. Kolitsidas, B. L. G. Jonsson, T. Empliouk, and G. A. Kyriacou, "A wideband switched beam antenna system for 5G femtocell applications," in *2017 IEEE International Symposium on Antennas and Propagation USNC/URSI National Radio Science Meeting*, July 2017, pp. 929–930.

[23] M. F. Wong, V. F. Hanna, O. Picon, and H. Baudrand, "Analysis and design of slot-coupled directional couplers between double-sided substrate microstrip lines," *IEEE Transactions on Microwave Theory and Techniques*, vol. 39, no. 12, pp. 2123–2129, Dec 1991.

[24] J. Shin and D. H. Schaubert, "A parameter study of stripline-fed vivaldi notch-antenna arrays," *IEEE Transactions on Antennas and Propagation*, vol. 47, no. 5, pp. 879–886, May 1999.

[25] P. S. Kildal, "Artificially soft and hard surfaces in electromagnetics," *IEEE Transactions on Antennas and Propagation*, vol. 38, no. 10, pp. 1537–1544, Oct 1990.

[26] H. Steyskal and J. S. Herd, "Mutual coupling compensation in small array antennas," *IEEE Transactions on Antennas and Propagation*, vol. 38, no. 12, pp. 1971–1975, Dec 1990.

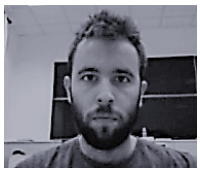

Petros Bantavis received the Diploma degree in electrical and computer engineering from Democritus University of Thrace Xanthi, Greece in 2016. In summer 2015 he was a trainee at KEMEA-Center for security studies, in Athens, Greece. He spent one year In Lab-STICC at ENSTA-Bretagne and UBO, Brest, France. Currently, he is working toward a Ph. D degree with IETR, Thales Alenia Space and Prodintec. His research interest include Lens antennas, antennas arrays, beamforming networks and full duplex systems.

Christos Kolitsidas (S12-M'18) received the Diploma and the M.Sc. degrees (with honors) in electrical and computer engineering from Democritus University of Thrace Xanthi, Greece in 2008 and 2012 respectively. In 2012 joint the department of Electromagnetic Engineering at KTH Royal Institute of Technology where he received his PhD degree. He has fulfilled his military service (2010-2011) as an officer in the Greek army in the corps of research and informatics and was discharged with the rank of reserve second lieutenant. He was the recipient of the best student paper award in 2008 at the Mediterranean Microwave Symposium and in 2014 at the Progress in Electromagnetic Research Symposium. In 2016 was the team mentor and project leader of the team "Trielectric" that won the 1^{st} prize in the student design contest held in the IEEE Antennas and Propagation Symposium.

In 2017, Mr. Kolitsidas spend four months as research visitor in the Cavendish Laboratory in Cambridge University UK working on experimental astrophysics. His research interest include antennas and antenna arrays, beamforming networks, energy harvesting, SIW technology, lens antennas and radio astrophysics for the global EoR experiment.

Mr. Kolitsidas is a member of the Technical Chamber of Greece.

Tzihat Empliouk received the Diploma and the M.Sc. degrees in electrical and computer engineering from Democritus University of Thrace Xanthi, Greece in 2004 and 2009 respectively. In 2012 started his PhD thesis in association with Microwave Lab of Democritus University of Thrace. His research interest include beamforming networks, antennas and antenna arrays and sixport networks. Mr. Empliouk is a member of the Technical Chamber of Greece.

George A. Kyriacou was born in Famagusta, Cyprus, on March 25, 1959. He received the Electrical Engineering diploma and Ph.D. degree both with honors) from the Democritus University of Thrace, Xanthi, Greece, in 1984 and 1988, respectively. Since January 1990, he has been continuously with the Department of Electrical and Computer Engineering, Democritus University of Thrace, where he is currently Professor and director of the Microwaves Laboratory. From 2005 to 2010 he has been Director of the Graduate Studies at the same Department. He has authored over 250 journal and conference papers and supervised 7 Ph.D. and 11 M.Sc. theses and more than 90 Diploma theses. His main research interests include microwave engineering, open waveguides and antennas in anisotropic media, software defined and cognitive radio, computational electromagnetics, and biomedical engineering. Dr. Kyriacou is member of IEEE since 1990 and senior member since 2000, also a member of the Technical Chamber of Greece and the European Microwave Association (EuMA).

Lars Jonsson (https://www.kth.se/profile/ljonsson/) received his Ph.D. degree in electromagnetic theory in 2001 from KTH Royal Institute of Technology, Stockholm, Sweden. He was a postdoctoral fellow at University of Toronto, Canada and a Wissenschaftlicher Mitarbeiter (postdoc) at ETH Zurich, Switzerland. 2006-2015, he was with the Electromagnetic Engineering Lab at KTH Royal Institute of Technology as an Associate Professor. He is a professor at KTH in the subject Electromagnetic fields since 2015. His research interests include electromagnetic theory in a wide sense, including scattering, antenna theory and nonlinear dynamics. Recently he has been working on physical bounds of antenna performance.

Marc Le Roy received the Ph.D. degree in electronics from the Université de Bretagne Occidentale (UBO), Brest, France in 1999. He is now assistant-Professor in the DIM team (Devices and Multiphysics Interfaces) at MOM research department (Microwave, Optoelectronics, Material) at the Lab-STICC (Laboratory of Sciences and Techniques of Information, Communication and Knowledge), a research unit associated with the Centre National de la Recherche Scientifique (UMR CNRS 6285). His research activities deal with the modelization and design of passive and active microwave devices such as nonuniform and periodic structures (PBG), filters, amplifiers, phase shifters, antenna, baluns... He currently investigates on the design of wideband tunable devices such as analog and digital phase shifters, negative group delay (NGD) or non-Foster active circuits.